

# Magnetic Properties of Chromium-Doped ZnO

T. A. Abdel-Baset<sup>1</sup> · Yue-Wen Fang<sup>2</sup> · Chun-Gang Duan<sup>2</sup> ·  
Mahmoud Abdel-Hafiez<sup>1,3,4</sup>

HPSTAR  
285\_2016

Received: 23 January 2016 / Accepted: 19 March 2016 / Published online: 30 March 2016  
© Springer Science+Business Media New York 2016

**Abstract** Cr-doped ZnO was synthesized by using a low-temperature co-precipitation technique producing Zn<sub>1-x</sub>Cr<sub>x</sub>O nanoparticles. The effects of the Cr concentration (0, 0.03, 0.05, and 0.07) on the structural, optical, and magnetic properties of ZnO were investigated by first-principles calculations, X-ray diffraction, scanning electron microscope, the optical spectroscopy (UV–Vis), and magnetization measurements. The results show that Cr atoms are substituted for Zn ions successfully. The Cr ions exhibited +3 valence state other than +2 valence state, which is supported by the fact of high-spin configurations of Cr ions in the first-principle calculations. X-ray diffraction confirms that the samples have a single-phase wurtzite structure with the main crystal size decreases with increasing dopant concentration. This decrease occurs due to the small ionic radius of Cr ions in compared to Zn ions. The morphology on the surface shows further that the samples had a spherical shape with an average particle size of 75 nm. The optical band gap of ZnO nanoparticles varies with Cr doping, which is attributed to the *s-d* and *p*

interaction. Introducing Cr into ZnO induces a strong magnetic moment. The estimated effective magnetic moment is very close to the magnetic moment obtained from total energy calculations.

**Keywords** ZnO · Magnetic properties

## 1 Introduction

The relation between semiconductors and magnetism has led to the next generation of magnetic semiconductors, where it is not the electron charge but the electron spin that carries information [1]. These diluted magnetic semiconductors (DMSs) are formed by the partial replacement of cations in a non-magnetic semiconductor by magnetic transition metal ions [2–5]. They are of keen potentials for various applications such as spintronics, spin-valve transistors [6], spin light-emitting diodes [7], and logic devices [8]. To realize these devices, it is necessary to develop semiconducting materials indicating a ferromagnetic behavior at room temperature. Ferromagnetic ZnO-based DMSs have been predicted to have Curie temperature above room temperature [9]. On the other hand, Coey and Chambers [10] have suggested that structurally perfect ZnO-based DMSs do not exhibit ferromagnetic order. Not only the magnetic dopants themselves but also vacancies are necessary for ferromagnetism. Due to the wide-band gap, ZnO is one of the most important functional semiconducting materials with a direct gap of 3.37 eV at room temperature. However, it has been increasingly explored accessing a wealth of phenomena including optoelectronics, UV light emitters, spintronics, and piezoelectric transducers [11–13]. It is reported that ZnO illustrates a large exciton binding energy of 60 meV, paving the way for an intense near-band-edge

✉ Mahmoud Abdel-Hafiez  
m.mohamed@hpstar.ac.cn

<sup>1</sup> Faculty of Science, Physics Department, Fayoum University, 63514 Fayoum, Egypt

<sup>2</sup> Key Laboratory of Polar Materials and Devices, Ministry of Education, East China Normal University, Shanghai 200241, China

<sup>3</sup> Center for High Pressure Science and Technology Advanced Research, Shanghai 201203, China

<sup>4</sup> Institute of Physics, Goethe University Frankfurt, 60438 Frankfurt/M, Germany

excitonic emission at room/higher temperatures [14]. There are several theoretical explanations of the origin of room temperature ferromagnetism in transition metal-doped ZnO: Dietl et al. [15] first predicted that a high  $T_c$  for transition metal-doped ZnO would require a large density of mobile holes inducing the ferromagnetic exchange interaction. However, a high concentration of a hole is difficult to achieve because of the compensation of the wide band gap ZnO. For technological applications, but also a better understanding of chromium doping, a precise control of the structural properties is as desired to understand their magnetic and optical properties.

Chromium is an important transition metal element dopant. It attracts lots of attention [16–19]. One of the reasons is that the radius parameter of  $\text{Cr}^{+3}$  is closer to that of  $\text{Zn}^{+2}$ , which either means that  $\text{Cr}^{+3}$  can easily penetrate into the ZnO crystal lattice or it can substitute the position of  $\text{Cr}^{+3}$  in the crystal ZnO [20]. Some studies reveal that the magnetic behavior of Cr-doped ZnO appears to be very sensitive to the deposition method. For example, Ueda et al. [21] did not observe any ferromagnetic behavior for Cr-doped ZnO film grown by pulse laser deposition, whereas Roberts et al. [22] prepared Cr-doped ZnO via magnetron sputtering. A ferromagnetic ordering at 9.5 % doping concentration was obtained. Furthermore, the results of Jin et al. [23] show no ferromagnetic behavior for a Cr-doped ZnO film at low temperatures even down to 3 K. Neither Lee et al. [24] did not find ferromagnetism in solgel synthesized  $\text{Zn}_{1-x}\text{Cr}_x\text{O}$  thin films. The calculated optical properties indicate that the optical energy gap increases after Cr doping [25]. Additionally, a strong absorption in the visible-light region is observed, which originates from the intraband transition of the Cr 3d bands and the conduction bands [25]. However, the experimental studies of their optical properties are still unknown.

The material synthesis is one of the key features for the development and realization of semiconductor-based spintronic applications. The ability to produce a high-quality

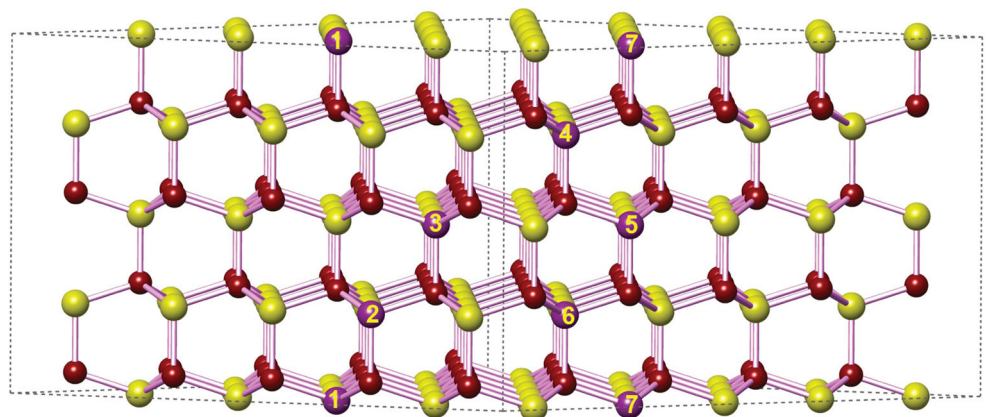
single-phase DMS is the driving factor to study DMS for spintronic applications. In this present work, Cr-doped ZnO nanoparticles were synthesized by a co-precipitation method. The effects of Cr concentration on ZnO nanoparticles were studied by X-ray diffraction (XRD), optical and magnetic measurements.

A 200-atom supercell of  $\text{Zn}_{1-x}\text{Cr}_x\text{O}$  applied by periodic boundary conditions is shown in Fig. 1. The  $\text{Cr}_{0.03}\text{Zn}_{0.97}\text{O}$  model can be obtained by replacing three Zn atoms with three Cr atoms. Five Zn atoms are replaced with five Cr atoms, which correspond to  $x = 0.05$ . For the case of  $\text{Cr}_{0.07}\text{Zn}_{0.93}\text{O}$ , seven Zn atoms are substituted by seven Cr atoms.

## 2 Method

All preparation steps like weighing, mixing, grinding, and storage were carried out in an Ar-filled glove-box, the  $\text{O}_2$  and  $\text{H}_2\text{O}$  level is less than 0.1 ppm. The preparation of  $\text{Cr}_x\text{Zn}_{1-x}\text{O}$  in a nanoparticle form is achieved by using the Co-precipitation technique. The following procedure was adopted. The  $\text{ZnCl}_2$  and NaOH solution are prepared separately and then mixed together. The solution was maintained in a first step at room temperature under stirring for 2 h. In a second step,  $\text{Zn}(\text{OH})_2$  has been heated up to 70 °C for 24 h to become dry. The dried ingots were heated up to 400 °C for 4 h. After that time period, the powder was left to cool down slowly to room temperature to get pure ZnO. To prepare mixed oxide dilute magnetic semiconductors, mixed solutions of  $\text{ZnCl}_2$  and  $\text{CrCl}_3$ , at the desired ratio were prepared. Then, the NaOH solution is added slowly to the mixed solution, and the process described above is repeated to obtain  $\text{Zn}_{1-x}\text{Cr}_x\text{O}$  nanoparticles. Particles shape and size distribution can be controlled by varying the atmosphere conditions inside evaporation chamber. Finally, the X-ray tests reveal that the obtained powder is composed of nanoparticles.

**Fig. 1** The schematic 200-atom supercell of  $\text{Zn}_{1-x}\text{Cr}_x\text{O}$ . Each oxygen atom (maroon sphere) is surrounded by four zinc atoms (yellow spheres) which forms a regular tetrahedron. The 7-purple spheres designate chromium atoms



The x-ray powder diffraction data were collected at room temperature using a Huber G670 Guinier imaging plate diffractometer with Co  $K\alpha$ -radiation and a Ge-111 monochromator. Scanning electron microscopy (SEM) images of the surface and crosssection of films were taken with a Leo Gemini 982 microscope. A Lambda 900 spectrometer from Perkin-Elmer Instruments was used to measure the optical transmittance in a wavelength range from 250 to 3000 nm. The magnetization measurements were performed by using a superconducting quantum interference device magnetometer (MPMS-XL5) from Quantum Design.

**Computational Details** A periodic  $5 \times 5 \times 2$  supercell containing 200 atoms, as shown in Fig. 1, is adopted in our calculations. An experimental dopant concentration can be achieved. Different dopant concentrations in the models were generated by substituting Zn ions by Cr ions. The first-principle calculations were performed by using the projector augmented wave formalism of density functional theory as implemented in the VASP package [27, 28]. We used a well-converged energy cutoff of 550 eV and a  $2 \times 2 \times 3$ -centered k-point grid for the total energy calculations. In order to add the on-site  $d$ - $d$  Coulomb interaction,  $U$ , and the on-site exchange interaction,  $J$ , to the generalized gradient approximation (GGA) Hamiltonian for transition-metal elements, we use typical values of  $U = 4.5$  eV and  $J = 0.5$  eV throughout our calculations [29, 30].

### 3 Results and Discussions

On the basis of the wurtzite ZnO unit cell, the  $5 \times 5 \times 2$  supercell containing 200-atoms is adopted for pure ZnO, as shown in Fig. 1. The crystal structure and orientation of the  $Zn_{1-x}Cr_xO$  nanostructure have been investigated by the XRD technique. The XRD pattern of the crystals is shown in Fig. 2. XRD results suggest that the  $Zn_{1-x}Cr_xO$  exhibit a hexagonal wurtzite structure with a preferred orientation of (101). The diffraction peaks corresponding to (002) and (100) planes of a ZnO hexagonal phase were also observed but with a different intensity ratio. The main crystallite size in the samples was estimated using Scherrer’s formula [26] given in Table 1. We find out that the lattice parameter  $a$  increases up to  $x = 0.05$  and then drops at 0.07-doping.

The microstructure of the  $Zn_{1-x}Cr_xO$  nanoparticles was investigated by SEM, as shown in Fig. 3. It clearly proofs that the structures of the investigated particles are crystals in form. In addition, Fig. 3 finds that the particles show a narrow size distribution due to their magnetic attraction exhibiting a partially sintered microstructure. The agglomeration of particles was related to many factors such as shape factor, surface area, porosity, and density. The investigated samples possess a uniform particle size which is listed

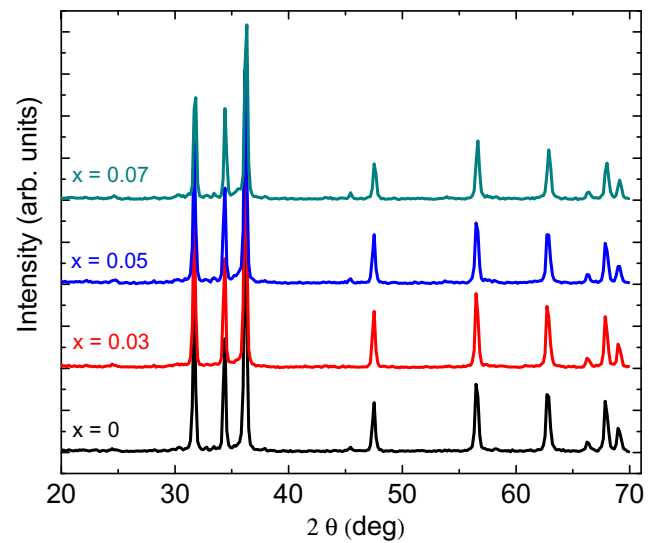


**Fig. 2** X-ray diffraction pattern of  $Zn_{1-x}Cr_xO$  nanoparticles.

in Table 1. It is worth mentioning that the most colloidal particles are electrically charged, e.g., most metal oxides have a surface layer of the metal hydroxide which is amphoteric and can become either positively or negatively charged.

The room temperature UV vs. absorption spectroscopy is a direct and simple method of probing the band structure of materials. The UV vs. absorption spectra of  $Zn_{1-x}Cr_xO$  nanoparticles is represented in Fig. 4a. The intensity of this band was dependent on the Cr concentrations, the direct optical energy band gap ( $E_g$ ) of  $Zn_{1-x}Cr_xO$  nanoparticles was determined from their UV vs. spectra according to the frequency dependence of the absorption coefficient,  $\alpha$ , (where  $\alpha = \text{absorbance}/\text{film thickness}$ ) and the optical band gap can be calculated using Tauc’s relation [31–34]. The variation of the absorption coefficient with photon energy is studied using the relation:

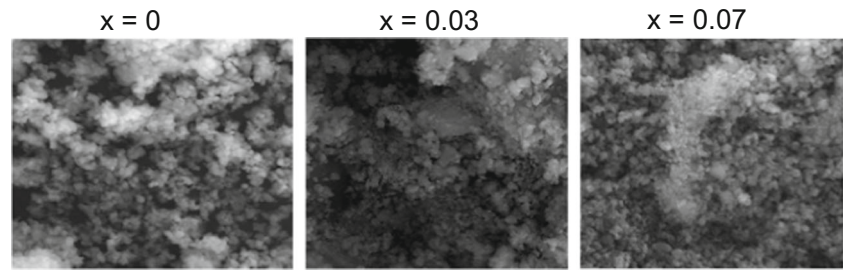
$$\alpha h\nu = A(h\nu - E_g)^{0.5}, \tag{1}$$

where  $h\nu$  is the photon energy,  $A$  is the probability parameter for transition, and  $E_g$  is the optical band gap. This implies that the optical band gap of the ZnO nanostructure has a direct optical transition. It is well known that direct transitions across the band gap are feasible between the valence and the conduction band edges in the  $k$ -space.

**Table 1** The calculated values of the lattice constants, the bond lengths, and the crystal size ( $D$ ) for  $Zn_{1-x}Fe_xO$  investigated at (101)

$x$	$a$	$c$	$c/a$	$D$ (nm)	$V$ (nm)	$E_g$	$E_u$
0	3.2	5.214	1.6	76.6	77	3.52	2.72
0.03	3.2	5.215	1.6	77.5	75.6	3.32	3.52
0.05	3.2	5.2	1.6	73.1	–	3.45	2.3
0.07	3.2	5.19	1.6	72.9	74.7	3.49	3.55

**Fig. 3** EM images for  $\text{Zn}_{1-x}\text{Cr}_x\text{O}$  samples, for Cr concentrations 0, 0.03 and 0.07 respectively



In this transition process, the total energy and momentum of the electron-photon system must be conserved. The direct band gap was obtained from the plots of  $(\alpha h\nu)^2$  vs.  $h\nu$  at  $RT$  enables us to estimate the  $E_g$  values by extrapolating the linear part of  $(\alpha h\nu)^2$  to zero as shown in the inset of Fig. 4b. The obtained optical band gap  $E_g$  values are tabulated in Table 1.

As can be seen that the  $E_g$  decreases with doping, which has been observed in doped II-IV compounds [35–37]. In terms of the  $sp-d$  spin exchange interaction between band electrons and the localized d electrons of the transition metal ions the cations is substituted.

The absorption coefficient near the fundamental absorption edge is exponentially dependant on  $h\nu$  and obeys the empirical Urbach relation. The Urbach energy can be calculated according to the following relation [38]:

$$\alpha = \alpha_0 \exp \left[ \frac{h\nu - E_I}{E_U} \right], \quad (2)$$

where  $E_I$  and  $\alpha_0$  are constants.  $E_U$  is the Urbach energy which is correlated to the width of the tails of localized states within the optical band gap. At the absorption edge, random internal electric fields will dominate the broadening of the excitation levels due to the lack of long-range order or presence of defects. Equation (2) describes the optical transition between occupied states in the valence band tail to unoccupied states of the conduction band edge. The  $E_U$  values were calculated from the slopes of the graphs shown

in Fig. 4c using the relationship  $E_U = (d \ln \alpha / h\nu)^{-1}$ , and are given in Table 1. The increase of  $E_U$  suggests that the atomic structural disorder of  $\text{Zn}_{1-x}\text{Cr}_x\text{O}$  increases by Cr doping.

Figure 5a presents the temperature dependence of the magnetization data measured up to 300 K with the magnetic field of 1 T applied parallel to the crystallographic  $c$  axis. For  $x = 0.07$  sample, the ferromagnetic transition is clearly seen with a peak at  $T = 48$  K, while the transition is shifted slightly to  $T = 52$  K in the case of  $x = 0.05$ . On the other hand, for  $x = 0.03$  and 0, doping this transition is smeared. However, we should mention while the magnetization of both samples  $M$  does increase as  $T$  is lowered, the  $M$ - $T$  curve is exactly what one would expect for a ferromagnet with a proper long-range order where a sharp transition at the ferromagnetic transition in the case of  $x = 0.07$  occurs. It is likely that the resulting phase in the nanoparticle of the investigated samples is ferromagnetic. Clearly, one can see that by increasing the Cr concentration to the ZnO, the magnetic moment increases with saturation of the magnetic moment at room temperature.

In Fig. 5b, we have shown a plot of inverse susceptibility  $1/\chi$  vs. temperature for the  $x = 0.07$  sample. In the paramagnetic region, the data between 300–130 K can be fitted to the Curie-Weiss law  $\chi = C/(T - \Theta)$ , where  $C$  is the Curie constant and  $\Theta$  is the Weiss temperature. The paramagnetic Curie temperature in both samples is nearly identical and positive. The  $\Theta$  for the  $x = 0.07$  sample is 229 K. From

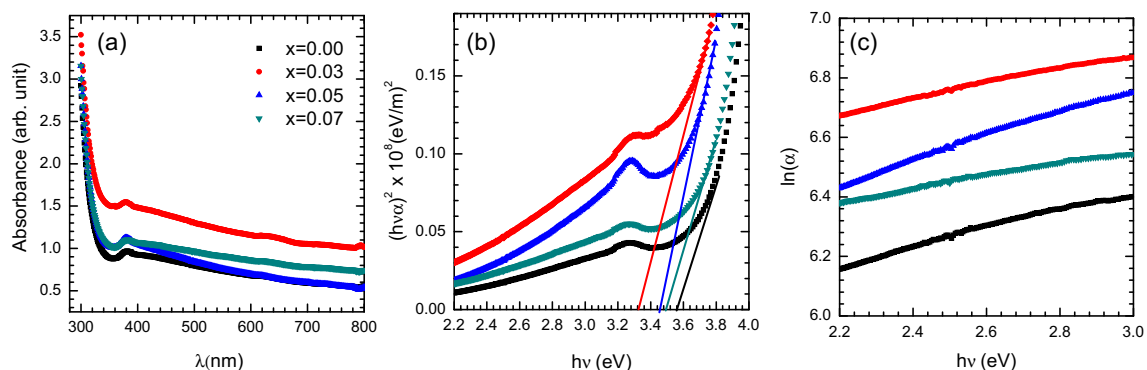
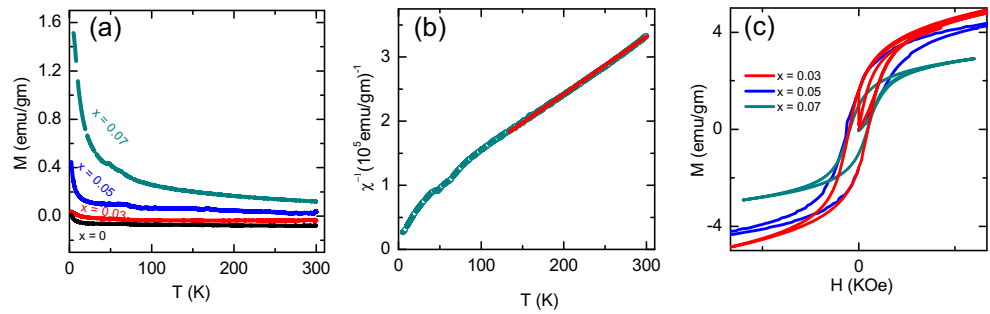


**Fig. 4** Panel a presents the main frame represents UV-vis absorption spectra. Panel b shows the plots of  $(\alpha h\nu)^2$  versus  $h\nu$ . Panel c  $\ln(\alpha)$  vs.  $h\nu$ , in which the Urbach energy of each particular doping is calculated from the slopes

**Fig. 5** **a** Magnetization vs. temperature of the four investigated samples under a magnetic field of 1 T. Panel **b** presents the inverse susceptibility  $1/\chi$  vs. temperature for  $x = 0.07$  sample. Panel **c** shows the magnetic hysteresis ( $M - H$ ) curves of  $x = 0.03, 0.05,$  and  $0.07$  measured at 2 K



the Curie constant  $C$ , we estimate the effective magnetic moment  $\mu_{eff}$  to be  $3.7\mu_B$ , this is very close to the magnetic moment  $3.66\mu_B$  obtained from total energy calculations. As shown in Fig. 6, a tetrahedral ligand field surrounding a central Cr ion (purple sphere) is formed, and drives to split states of  $d$  symmetry into two sets of two and three states each by the crystal-field splitting. In this tetrahedral crystal field induced by the oxygen anions,  $d_{xy}, d_{yz},$  and  $d_{xz}$  orbitals are raised in energy relative to the  $d_{x^2-y^2}$  and  $d_{z^2}$  orbitals. The results in our first-principle calculations show that chromium ion adopt a high spin configuration at  $t_{2g}^2 e_g^2$  with a +3 valence state. In the perfectly tetrahedral environment, two  $e_g$  electrons can occupy two of  $d_{xy}, d_{yz}$  or  $d_{xz}$  orbitals with equal probability. However, as confirmed by our observations in Fig. 5, structural disorder was increased by Cr doping, which may lower the symmetry and further have effects on the electron occupations. This establishes that the paramagnetic state of our samples have not much affected by the particle size. This is indeed interesting since our investigated samples are chemically identical and have nearly an identical paramagnetic state, but the  $x = 0.03$  sample becomes a ferromagnet with abroad transition while the  $x = 0.07$  and  $0.05$  samples have a lower moment and leading a sharp ferromagnetic transition.

Apart from the above calculations, we also performed total energy calculations for other two structure

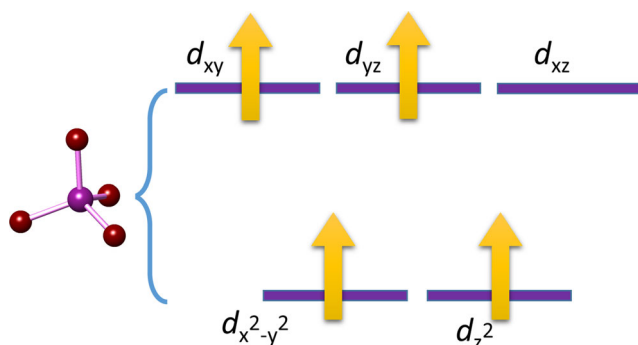


**Fig. 6** Tetrahedral crystal field generated by oxygen anions. Chromium ion adopts a high spin configuration at  $t_{2g}^2 e_g^2$  with a +3 valence state

configurations. One is a close configuration [39], in which sites 1 and 2 (Fig. 1) are occupied by Cr atoms. While the other one is a “separated” configuration [39] where Zn atoms at sites 1 and 3 (Fig. 1) are replaced by Cr atoms. For both configurations, we have computed the relative energies of the ferromagnetic and antiferromagnetic structures. Our calculations show that the separated configuration is more energetically favorable than the separated one by around 90 meV. This result reveals that the Cr ions prefer distributing themselves evenly throughout the lattice, rather than cluster together in the samples. Consequently, the magnetism derived from Cr clusters can be excluded. On the other hand, it is well known that the pure ZnO nanoparticles are paramagnetic materials, which are also confirmed by our experiments. Cr-doped ZnO exhibits a clearly magnetic hysteresis loop. As reported by Xing et al. that the appearance of ferromagnetism in transition metal-doped ZnO might be due to the increase of the number of defects and oxygen vacancies [40]. On the other hand, theoretically, Chu et al. proof that ferromagnetism could be induced by the exchange interaction between transition metal ions and O ion spin moments [41]. One can see that there is an enhancement of the magnetic moment in the  $x = 0.07$  nanoparticle sample in contrast to  $x = 0$  sample as revealed through the magnetization. It is apparent that there is a proper long-range ferromagnetic order in the  $x = 0.07$  sample which is sharper than the  $x = 0.03$  and 0-doping sample. The reason can also be seen in the hysteresis curve shown in Fig. 5c. The magnetic field varies from  $-3$  to  $+3$  T. The  $x = 0.03$  sample shows a small hysteresis loop which closes at  $\approx 600$  Oe. In addition, the magnetization of  $x = 0.03, 0.05,$  and  $0.07$  samples is saturated at a fields of 2.7, 4.5, 5.2 kOe, respectively with another signature of the resulting ferromagnetic state.

The observed ferromagnetism is mainly due to the Cr ions substituting Zn in the ZnO host lattice and not due to Cr metal cluster-like phases. Thus, introducing Cr into ZnO induces a strong magnetic moment without any distortion in the geometrical symmetry. It also reveals the ferromagnetic coupling. It is interesting to note that the reduction in the moment of  $x = 0.03$  sample compared to  $x = 0.07$  might

occur due to large disordered spins in the surface as well due to grain boundaries that constitute a good fraction of the nanosample.

#### 4 Summary

To summarize, we find that there is a rather strong enhancement of the ferromagnetic moments in the  $x = 0.07$  sample in contrast to  $x = 0.03$  sample, which is confirmed by magnetic measurement and first-principle calculations. As  $x$  increases to 0.07, the magnetization decreases monotonously. The optical band gap decreases with doping. Introducing Cr into ZnO induces a strong magnetic moment without any distortion in the geometrical symmetry and it also reveals that the ferromagnetic coupling, which plays an important role in prompting its practical application in the future.

**Acknowledgments** The works in ECNU and IOP of CAS are supported by the Natural Science Foundation of China (Nos. 61125403, 11374011, and 91221303), the Ministry of Science and Technology of China (973 projects: Grants Nos. 2011CBA00110, 2012CB821400, 2013CB922301, and 2014CB921104). The work by M.A. was supported by the MO 3014/1-1 of the DFG.

#### References

- Sato, K., Katayama-Yoshida, H.: *Jpn. J. Appl. Phys.* **39**, 555 (2000)
- Liu, X.C., Shi, E.W., Chen, Z.Z., Zhang, T., Zhang, Y., Chen, B.Y., Huang, W., Liu, X., Song, L.X., Zhou, K.J., Cui, M.Q.: *Appl. Phys. Lett* **92**, 042502 (2008)
- Roberts B.K., Pakhomov A.B., Krishnan K.M.: *Appl. Phys. Lett.* **103**, 07D133 (2008)
- Liu, G.L., Cao, Q., Deng, J.X., Xing, P.F., Tian, Y.F., Chen, Y.X., Yan, S.S., Mei, L.M.: *Appl. Phys. Lett* **90**, 052504 (2007)
- Xing, G.Z., Yi, J.B., Tao, J.G., Liu, T., Wong, L.M., Zhang, Z., Li, G.P., Wang, S.J., Ding, J., Sum, T.C., Huan, C.H.A., Wu, T.: *Adv. Mater.* **20**, 3521 (2008)
- Tanaka, M., Higo, Y.: *Phys. Rev. Lett* **87**, 26602 (2001)
- Pearnton, S.J., Abernathy, C.R., Overberg, M.E., Thaler, G.T., Norton, D.P., Theodoropoulou, N., Hebard, A.F., Park, Y.D., Ren, F., Kim, J., Boatner, L.A.: *J. Appl. Phys* **93**, 1 (2003)
- Wang, Y.Z., Liu, H., Li, Z.Q., Zhang, X.X., Zheng, R.K., Ringer, S.P.: *Appl. Phys. Lett* **89**, 042511 (2006)
- Sato, K., Katayama-Yoshida, H.: *Jpn. J. Appl. Phys* **40**, L334 (2001)
- Coey, J., Chambers, S.A.: *MRS Bull* **33**, 1053 (2008)
- Xu, W.Z., Ye, Z.Z., Zeng, Y.J., Zhu, L.P., Zhao, B.H., Jiang, L., Lu, J.G., He, H.P., Zhang, S.B.: *Appl. Phys. Lett* **88**, 173506 (2006)
- Tu, Z.C., Hu, X.: *Phys. Rev. B* **74**, 035434 (2006)
- Mitra, P., Chatterjee, A.P., Maiti, H.S.: *Mater. Lett.* **35**, 33 (1998)
- Zu, P., Tang, Z.K., Wong, G.K.L., Kawasaki, M., Ohtomo, A., Koinuma, H., Segawa, Y.: *Solid State Commun* **103**, 459 (1997)
- Dietl, T., Ohno, H., Matsukura, F., Cibert, J., Ferrand, D.: *Science* **207**, 1019 (2000)
- Vijayalakshmi, K., Sivaraj, D.: *RSC Adv* **5**, 68461 (2015)
- Palvinder Kaur, P., Pandey, S.K., Kumar, S., Negi, N.S., Chen, C.L., Rao, S.M., Wu, M.K.: *Appl Nanosci* **5**, 975 (2015)
- Zhuge, L.J., Wu, X.M., Wu, Z.F., Chen, X.M., Meng, Y.D.: *Scripta Mater* **60**, 214 (2009)
- Schneider, L., Zaitsev, S.V., Jin, W., Kompch, A., Winterer, M., Acet, M., Bacher, G.: *Nanotechnology* **20**, 135604 (2009)
- Wang, B.Q., Iqbal, J., Shan, X.D., Huang, G.W., Fu, H.G., Yu, R.H., Yu, D.: *Mater. Chem.Phys.* **113**, 103 (2009)
- Ueda, K., Tabata, H., Kawai, T.: *Appl. Phys. Lett* **79**, 988 (2001)
- Roberts B.K., Pakhomov A.B., Shuthanandan V.S., Krishnan K.M.: *J. Appl.Phys.* **97**, 10D3103 (2005)
- Jin, Z., Fukumura, T., Kawasaki, M., Ando, K., Saito, H., Sekiguchi, T., Yoo, Y.Z., Murakami, M., Matsumoto, Y., Hasegawa, T., Koinuma, H.: *Appl. Phys. Lett* **78**, 3824 (2001)
- Lee, H.J., Jeong, S.Y., Hwang, J.Y., Cho, C.R.: *Europhysics Lett* **64**, 797 (2003)
- Li, L., Wang, W., Liu, H., Liu, X., Song, Q., Ren, S.: *J. Phys. Chem. C* **113**, 8460 (2009)
- Cullity, B.D.: *Elements of X-ray Diffractions*, Addition-Wesley, Reading, MA Publishing house, 102 (1978)
- Kresse, G., Hafner, J.: *Phys. Rev. B* **47**, 558 (1993)
- Kresse, G., Hafner, J.: *Phys. Rev. B* **49**, 14251 (1994)
- Gopal, P., Spaldin, N.A.: *Phys. Rev. B* **74**, 094418 (2006)
- Cococcioni, M., de Gironcoli, S.: *Phys. Rev. B* **71**, 035105 (2005)
- Reddeppa, N., Sharma, A.K., Rao, V.V.R.N., Chen, W.: *Microelectron. Eng* **112**, 57 (2013)
- Mahmoud, W.E.: *Euro. Polym. J* **47**, 1534 (2011)
- Mahmoud, W.E., Al Ghamdi, A.A., Al Agel, F.: *Polym. Adv. Technol* **22**, 2055 (2011)
- Mahmoud, W.E., Shirbeeney, W., Al Ghamdi, A.A., Al Heniti, S.: *Appl. Polym. Sci* **125**, 339 (2012)
- Fitzgerald, C.B.: *Appl. Surf. Sci.* **247**, 493 (2005)
- Lee, Y.R., Ramdas, A.K., Aggarwal, R.L.: *Phys. Rev. B* **38**, 10600 (1998)
- Bylsma, R.B., Becker, W.M., Kossut, J., Debska, U., Short, D.Y.: *Phys. Rev. B* **33**, 8207 (1986)
- Urbach, F.: *Phys. Rev.* **92**, 1324 (1953)
- Spaldin, N.A.: *Phys. Rev. B* **69**, 125201 (2004)
- Xing, G.Z., Yi, J.B., Wang, D.D., Liao, L., Yu, T., Shen, Z.X., Huan, C.H.A., Sum, T.C., Ding, J., Wu, T.: *Phys. Rev. B* **79**, 174406 (2009)
- Chu, D.W., Zeng, Y.P., Jiang, D.L.: *Solid State Commun* **143**, 308 (2007)